A total synthetic approach to CRISPR/Cas9 genome editing and homology directed repair

Sara E. DiNapoli[1,2 *], Raul Martinez-McFaline[1,2 *], Caitlin K. Gribbin[1,2*], Paul Wrighton[3], Courtney A. Balgobin[1,2], Isabel Nelson[1,2], Abigail Leonard[1,2], Carolyn R. Maskin[1,2], Arkadi Shwartz[3], Eleanor D. Quenzer[3], Darya Mailhiot[4], Clara Kao[5], Sean C. McConnell[5], Jill L.O. de Jong[5], Wolfram Goessling[3,6], Yariv Houvras[1,2,7 **]

1. Department of Surgery, Weill Cornell Medical College, New York Presbyterian Hospital, New York, NY, USA
2. Meyer Cancer Center, Weill Cornell Medical College, New York Presbyterian Hospital, New York, NY, USA
3. Department of Medicine, Division of Genetics, Brigham and Women's Hospital, Harvard Medical School, Boston, MA, USA
4. Department of Surgery, Animal Resources Center, University of Chicago, Chicago, IL, USA
5. Department of Pediatrics, University of Chicago, Chicago, IL, USA
6. Division of Gastroenterology, Massachusetts General Hospital, Harvard Medical School, Boston, MA, USA
7. Department of Medicine, Weill Cornell Medical College, New York Presbyterian Hospital, New York, NY, USA

* These authors contributed equally to this work.

** Correspondence and requests for materials should be addressed to Y.H. (email: yah9014@med.cornell.edu).

ABSTRACT

CRISPR/Cas9 has become a powerful tool for genome editing in zebrafish that permits the rapid generation of loss of function mutations and the knock-in of specific alleles using DNA templates and homology directed repair (HDR). We compared synthetic, chemically modified sgRNAs to in vitro transcribed sgRNAs and demonstrate the increased activity of synthetic sgRNAs in combination with recombinant Cas9 protein. We developed an in vivo genetic assay to measure HDR efficiency and we utilized this assay to optimize the design of synthetic DNA templates to promote HDR. Utilizing these principles, we successfully performed knock-in of fluorophores at multiple genomic loci and demonstrate transmission through the germline at high efficiency. We demonstrate that synthetic HDR templates can be used to knock-in bacterial nitroreductase (*ntr*) to facilitate lineage ablation of specific cell types. Collectively, our data demonstrate the utility of combining synthetic sgRNAs and dsDNA templates to perform homology directed repair and genome editing in vivo.

INTRODUCTION

CRISPR/Cas9 has been used for a wide range of experimental applications, and zebrafish has been a key model organism to test and validate strategies for genome editing {Jao, 2013 #1}{Shah, 2015 #3}. Repair of CRISPR-generated double-stranded breaks (DSBs) by non-homologous end joining (NHEJ) leads to insertions and deletions (indels) which may result in loss of function of the targeted gene product. By supplying an exogenous DNA template, DSBs can be repaired through homology directed repair (HDR), allowing for precision genome editing, including base pair changes and insertion of protein tags. Prior studies reporting genome editing in zebrafish have used single-stranded donor oligonucleotides (ssODN) to knock-in short DNA sequences {Hruscha, 2013 #34}{Burg, 2018 #35}{Irion, 2014 #7}{Hwang, 2013 #42} or plasmid-based donor vectors to knock-in fluorophores {Auer, 2014 #6}{Hisano, 2015 #36}{Hoshijima, 2016 #9}{Ota, 2016 #38}{Kimura, 2014 #11}. The efficiency of transmitting fluorophore

knock-in through the germline has varied widely. We reasoned that the use of synthetic reagents could permit a comparison of approaches and rational optimization. Reports have described an increased efficiency of CRISPR/Cas9 targeting in human cells using chemically modified synthetic sgRNAs {Hendel, 2015 #12}{Rahdar, 2015 #13}. We evaluated synthetic sgRNAs and found that they outperform conventional in vitro transcribed (IVT) sgRNAs. We used these sgRNAs in combination with synthetic DNA templates and we developed an assay for HDR in zebrafish utilizing an *mitfa* mutant, b692. This assay allowed us to quantitatively compare multiple templates for HDR and correlate phenotypic and molecular efficiency. We performed precise genomic editing and generated in-frame gene fusions with fluorophores using synthetic reagents, including linear dsDNA templates. Knock-in alleles were transmitted through the germline at efficiencies of 14–25%. Finally, we used HDR to target bacterial nitroreductase (*ntr)* to the liver-specific gene *fabp10a* to perform lineage ablation of hepatocytes. These results demonstrate that the combination of synthetic sgRNAs and dsDNA templates result in efficient genome editing in zebrafish.

MATERIALS AND METHODS

sgRNA and HDR template sequence selection

Gene-specific sgRNAs sequences were selected using a combination of prediction tools including sgRNA Scorer 1.0 and 2.0{Chari, 2015 #14}{Chari, 2017 #15}, GuideScan{Perez, 2017 #16}, or CRISPRz{Varshney, 2016 #17}. We selected sgRNA sequences with zero predicted off targets with one base pair mismatch. Design principles for HDR templates included a mutated sgRNA recognition sequence, incorporation of barcoded nucleotides, homology arms, and incorporation of heterologous DNA sequence encoding EGFP or mScarlet. HDR templates were ordered as gBlock Gene Fragments (Integrated DNA Technologies [IDT]). For single stranded DNA templates Ultramer DNA Oligonucleotides (IDT) were used. gBlocks

were resuspended in nuclease-free water to a concentration of 50 ηg/μL and stored at -20ºC.

Preparation of sgRNAs

Synthesis of IVT sgRNAs was performed from dsDNA templates (gBlock, IDT) using the SureGuide gRNA Synthesis Kit (Agilent, 5190-7719). Templates contained a T7 promoter and GG dinucleotide to promote transcription (TAATACGACTCACTATAGG), a 20bp target site without PAM site, and a composite crRNA/tracrRNA single guide RNA sequence (sgRNA) (GTTTTAGAGCTAGAAATAGCAAGTTAAAATAAGGCTAGTCCGTTATCAACTTGAAAAAGTGGCACCGAGTCGGTGCTTTT). 50ηg of dsDNA template (10ηg/μL) was in vitro transcribed in a 25μL reaction and incubated at 37ºC for 3–4 hours. Following DNAse digestion sgRNAs were column-purified and eluted in H_2O per the manufacturer's (Agilent) instructions. Concentration was determined using a Nanodrop spectrophotometer and 200ηg of the sgRNA was visualized on an agarose gel for quality control.

Gene-specific crRNAs were synthesized by IDT as Alt-R® CRISPR-Cas9 crRNAs. A bipartite synthetic sgRNA was heteroduplexed using gene-specific crRNAs and a tracrRNA according to manufacturer recommendations. For simplicity the bipartite synthetic sgRNA is referred to as a synthetic sgRNA throughout the manuscript.

Microinjection

For global editing with a single sgRNA, 250ρg sgRNA and 500ρg recombinant Cas9 protein (rCas9, PNA Bio CP01) were injected into the yolk of one-cell stage embryos. Cas9 nickase (D10A Cas9 nickase protein with NLS, PNABio CN01) was purchased from PNA Bio. To generate deletions, 250ρg sgRNA 1, 250ρg sgRNA 2, and 500ρg rCas9 were injected into the yolk of one-cell stage embryos. For HDR injections, 250ρg

sgRNA, 500ρg rCas9, and 37.5ρg HDR template were injected into one-cell stage embryos. Throughout the manuscript rCas9 refers to recombinant Cas9 protein.

Assessment of gene editing efficiency

Genomic DNA was isolated from individual embryos (24–48 hours post fertilization [hpf]) using DirectPCR Lysis Reagent (Viagen, 102-T) supplemented with Proteinase K at 20μg/mL (Qiagen, 158920). Samples were incubated at 55°C for 60 min followed by 85˚C for 45 min. Genomic DNA was PCR amplified using specified primers (Supplementary Table). 8 μL of PCR product was mixed with 1.6μL NEB Buffer 2 and 6.4μL of water and was incubated at 95ºC for 5 minutes followed by cooling from 95ºC–85ºC at -2°C/second and 85–25°C at -0.1°C/second. Following hybridization, the DNA was subject to T7 endonuclease (T7EI) digestion with 2U of T7EI endonuclease (New England BioLabs [NEB], M0302) and 1 hour incubation at 37ºC. The reaction product was visualized on a 2% agarose gel.

For clonal analysis, the PCR product was cloned into pCRII-TOPO (Invitrogen, K460001) and Sanger sequenced (Genewiz). Sequences were compared to reference genome and non-targeting controls to identify indels using CrispRVariants{Lindsay, 2016 #18} and MacVector (Version 15.5).

For CRISPR-STAT analysis, sperm samples from potential founders were collected with 10μL capillary tubes as previously described, and then followed the HOTShot method with 25μL alkaline lysis buffer to prepare DNA templates{Draper, 2009 #19}{Meeker, 2007 #20}. Tail clips were prepared similarly. The CRISPR-STAT protocol was used to perform fluorescence-based genotyping{Carrington, 2015 #21}. Primers sequences used for the CRISPR-STAT assay were *slc6a15* FOR, tgtaaaacgacggccagtGGCCACGACCTACTACTGGTAT, which includes (lowercase) M13 tag for binding to a fluorescent-labeled M13 primer; and *slc6a15* REV, gtgtcttTATAGATGCTGCGTCACGTTTC, which include the (lowercase) ‘PIG tail’ tag

150 that helps ensure uniform product size, via Taq adenylation{Holleley, 2009 #22}.
151 Relative amounts of each uniquely sized PCR product (>100 bp and >100 peak height)
152 were calculated with area under the curve measurements using Applied Biosystems
153 Peak Scanner software.
154
155 For assessment of deletions, genomic DNA was PCR amplified using primers that
156 flanked the deletion sgRNAs. PCR products were purified (Qiagen, 28104), Sanger
157 sequenced, and compared to the reference genome.
158
159 **Analysis of HDR efficiency by next-generation sequencing**
160
161 For analysis of HDR efficiency by next-generation DNA sequencing, 50ηg of PCR
162 amplicon was converted into blunt ends using T4 DNA polymerase (New England
163 Biolabs, NEB) and *E. coli* DNA polymerase I Klenow fragment (NEB). Libraries were
164 prepared using the Kapa LTP Library Preparation Kit (Roche). Multiple indexing
165 adapters were ligated to the ends of the DNA fragments. Ligation reaction products
166 were purified by AMPure XP beads (NEB) to remove unligated adapters and quantified
167 using Qubit (Thermo Fisher Scientific) and Bioanalyzer DNA chip (Agilent). Indexed
168 sample libraries were normalized, pooled, and sequenced using the Illumina HiSeq4000
169 sequencer at 2x50 cycles. Reads were aligned to the zebrafish genome (GRCz10)
170 using the Star aligner{Dobin, 2013 #23} and visualized using Integrative Genome
171 Browser (IGV) {Thorvaldsdottir, 2013 #24}{Robinson, 2011 #25}.
172
173 **Imaging**
174
175 Micrographs of whole embryos and larval animals were taken with a Zeiss Discovery V8
176 stereomicroscope (Zeiss) equipped with epifluorescence and appropriate filters. Live
177 imaging of fluorescent larvae was acquired with a Zeiss LSM800 laser scanning
178 confocal microscope (Zeiss). For melanocyte counting, 48hpf embryos were visualized

179 under the stereoscope and binned into 4 categories (WT, >101, 51–100, or 0–50
180 melanocytes). Individuals scoring embryos were blinded to the experimental conditions.
181
182 **Hepatocyte ablation**
183 HDR injection mixes were made as described above. Approximately 2 ηL of mix was
184 injected into the cell of one-cell stage wild-type (Tu) embryos. At 4–6 days post
185 fertilization (dpf), embryos were screened by confocal microscopy for mosaic mScarlet
186 expression localized to the liver, and positive larvae were raised to adulthood. F_0 adults
187 were outcrossed with wild-type (TL) fish, and the F_1 embryos were screened by confocal
188 microscopy for mScarlet positive livers. Positive larvae were divided and treated with
189 either 0.2% dimethylsufoxide (DMSO; Sigma Aldrich) or 10 μM metronidazole (Mtz;
190 Sigma Aldrich 443-48-1) in egg water. After 24 hours, the larvae were washed,
191 anesthetized with 0.16 mg/mL tricaine-S (MS 222; Western Chemical, Inc.), and
192 immobilized in 0.8% low melt point agarose (Invitrogen) on glass-bottom dishes
193 (MatTek). Imaging was performed using a Nikon Ti2 inverted microscope equipped with
194 a Yokogawa CSU-W1 spinning disk confocal unit and a Zyla 4.2 PLUS sCMOS camera
195 (Andor), using CFI Plan Apochromat Lambda 10x NA 0.45 and 20x NA 0.8 objectives.
196 Larvae were recovered from the agarose, allowed to recover in the absence of drug for
197 48 hours, and imaged again.
198
199
200 **Zebrafish husbandry**
201
202 Zebrafish strains were maintained according to established guidelines{Westerfield, 2007
203 #33}. Wild-type animals were from the AB background except when indicated.
204 Experiments were performed in accordance with the recommendations in the Guide for
205 the Care and Use of Laboratory Animals of the National Institutes of Health. All of the
206 animals were handled according to approved institutional animal care and use
207 committee (IACUC) protocols of the respective institutions.
208

209 **RESULTS**

210

211 **Synthetic sgRNAs lead to highly efficient induction of indels**

212

213 In order to directly compare editing efficiencies generated by synthetic sgRNA versus
214 IVT sgRNA), we targeted tyrosinase (*tyr*), a gene required for melanin synthesis. Wild-
215 type zebrafish embryos were microinjected at the one-cell stage with recombinant Cas9
216 protein (rCas9) complexed with either synthetic sgRNA (IDT, Alt-R®) or with laboratory-
217 synthesized IVT sgRNA. Embryos were scored for melanocyte number at 48 hours post
218 fertilization (hpf) and divided into phenotypic categories representing the degree of gene
219 editing (Figure 1A). We find that the synthetic sgRNA leads to a significantly increased
220 fraction of embryos with fewer melanocytes than the IVT sgRNA (Figure 1B). Higher
221 doses of synthetic sgRNA produce an increase in the fraction of phenotypically edited
222 embryos. Only synthetic sgRNAs were capable of producing large numbers of embryos
223 with high phenotype. In order to characterize the molecular alterations of synthetic
224 sgRNA injected embryos, we performed a clonal analysis. We find that 10/10 clones
225 from a synthetic sgRNA injected high-phenotype embryo contain indels, as compared
226 with 7/10 clones from an IVT sgRNA injected high-phenotype embryo; we also observe
227 significant differences in the indel spectrum (Figure 1C). We found comparable
228 differences between synthetic and IVT sgRNAs at two additional loci, *slc24a5* and
229 *slc45a2* (Supplementary Figure 1). Injection of synthetic sgRNAs leads to highly
230 penetrant phenotypes in F_0 larvae that develop into adults that phenocopy established
231 germline mutants{Sheets, 2007 #26} (Supplementary Figure 2). We find that pairs of
232 synthetic sgRNAs are able to induce deletions spanning up to 124kB in genomic DNA
233 and that the efficiency of generating deletions varies with size (Supplementary Figure
234 3). Taken together, these data indicate that combined use of rCas9 protein with
235 synthetic sgRNAs leads to penetrant phenotypes and a broad spectrum of gene-specific
236 edits.

237

238 To assess the extent of germline transmission of edited alleles, we applied CRISPR-
239 STAT fluorescence-based genotyping to F_0 founders and progeny{Carrington, 2015
240 #21}. Sperm samples were collected from F_0 founders injected with rCas9 and synthetic
241 sgRNA targeting *slc6a15* at the one-cell stage. Results reveal mutant alleles containing
242 indels as the major peaks, with additional minor peaks corresponding to wild-type and
243 mutant alleles, indicating a high efficiency of CRISPR-induced mutagenesis in the
244 germline (Supplementary Figure 4). We identified five distinct alleles that were
245 transmitted to F_1 progeny (Supplementary Figure 4B-F). The frequencies of observed
246 CRISPR-induced indels in F_1 progeny were similar to those found in the sperm of the F_0
247 founder (Supplementary Figure 4G). These findings are consistent with high levels of
248 somatic mosaicism and confirm that F_0 sperm samples accurately predict the specific
249 mutations transmitted to F_1 progeny. These data demonstrate that CRISPR-induced
250 indels created with synthetic sgRNAs are found in the germline of founders and are
251 efficiently transmitted to F_1 progeny.
252
253 **A genetic assay for homology-directed repair**
254
255 To develop a quantitative assay for optimizing HDR in zebrafish, we sought to target a
256 locus that could provide phenotypic and molecular data on allele conversion. We initially
257 examined the widely used *mitfa*(w2) mutant, which lacks melanocytes{Lister, 1999 #27}.
258 Unexpectedly, injection of rCas9 complexed with a synthetic sgRNA targeting the
259 mutation site in w2 resulted in restoration of pigmented melanocytes (Supplementary
260 Figure 5). We presume that indels caused by targeting the *mitfa*(w2) mutation site
261 (Q113Stop) lead to in-frame deletions and restore protein function since this region of
262 the protein is relatively unstructured. We next examined the *mitfa*(b692) mutant, which
263 lacks melanocytes and harbors a mutation leading to a Ile215Ser substitution{Lister,
264 2001 #28}. We find that a synthetic sgRNA targeting the *mitfa*(b692) mutation site does
265 not restore pigmented melanocytes (Supplementary Figure 5). Therefore, we used
266 *mitfa*(b692) to develop a quantitative phenotypic and molecular assay for optimizing
267 HDR.

268

269 Using the b692-HDR assay we examined a range of synthetic templates to optimize
270 HDR efficiency. *mitfa*(b692) embryos were microinjected with rCas9, synthetic sgRNA,
271 and synthetic DNA templates designed to restore the wild-type *mitfa* sequence and
272 gene function. Microinjected embryos were scored at 48hpf for phenotypic evidence of
273 melanocytes, indicative of allele conversion and mitfa function (Figure 2A). Melanocytes
274 were not identified in uninjected embryos or in embryos injected with non-targeting
275 sgRNA. HDR templates were designed to feature multiple barcoded nucleotides and
276 mutated sgRNA recognition sequence, enabling unambiguous detection by sequencing
277 and prevention of re-cleavage by rCas9. We found that a 951bp, double-stranded linear
278 DNA template with an asymmetric sgRNA site located at the 3' end leads to a
279 reproducible 9% rate of phenotypic rescue in *mitfa*(b692) embryos (Figure 2B).
280 Melanocyte-positive embryos were subject to allele-specific PCR and Sanger
281 sequencing to confirm precise HDR (Figure 2C-D).
282

283 We examined DNA templates that differ in length, single vs. double stranded DNA,
284 linear vs. circular templates, and the symmetry of the sgRNA position within the
285 template (Figure 2E). We find that both longer (2kB) and shorter (318bp, 76bp) DNA
286 templates led to a decrease in HDR efficiency. Asymmetric positioning of sgRNA sites
287 led to higher efficiency than symmetric positioning. We tested an IVT sgRNA in
288 combination with rCas9 and the optimal 951bp linear dsDNA template and found no
289 appreciable HDR. Our data indicates that HDR efficiency is maximal with dsDNA
290 templates and synthetic sgRNA and that HDR is sensitive to template length and
291 sgRNA site symmetry within the HDR template.
292

293 Using the b692 assay we examined multiple reagents and conditions reported to
294 improve HDR efficiency in other model systems (Figure 2E). The addition of a second
295 sgRNA site in the optimal 951bp template reduced HDR efficiency to < 1%. We cloned
296 the 951bp template into a TopoTA plasmid vector and microinjected a circular plasmid
297 into zebrafish. This plasmid-based template also failed to lead to measurable HDR in

298 b692 embryos. In light of prior studies reporting increased HDR efficiency with the use
299 of catalytically-mutated Cas9 (nickase Cas9) {Richardson, 2016 #29}, we altered the
300 951bp DNA template to allow us to test this approach. Microinjection of paired sgRNAs
301 and recombinant nickase Cas9 failed to lead to measurable HDR in b692 embryos.
302 Based on reports that small molecule inhibitors of poly (ADP-ribose) polymerase
303 (PARP) stimulate HDR efficiency {Anantha, 2017 #32}, we performed microinjection of
304 the 951bp template and a PARP inhibitor, but did not observe any measurable HDR
305 efficiency. Finally, we examined the effect of cleaving the ends of the linear 951bp
306 template with a restriction enzyme (ISce-I), but we did not observe measurable HDR
307 under this condition.
308
309 **Melanocyte restoration in b692 assay correlates with molecular efficiency**
310
311 Using the b692-HDR assay we sought to measure the molecular efficiency of genome
312 editing and correlate DNA template integration with melanocyte number. To this end, we
313 performed single-cell injections in a large cohort of b692 embryos using the optimized
314 reagents described: rCas9, synthetic b692 sgRNA, and 951bp linear dsDNA template.
315 Embryos were scored for the presence of melanocytes at 48hpf and binned by
316 phenotype into four categories: high-, medium-, low-, and no-editing. Uninjected
317 embryos were included as a negative control. Genomic DNA was extracted from pools
318 of five embryos in each category, and exon 7 was amplified by PCR. Amplicons from
319 each group were subjected to next-generation sequencing. We find that that the
320 efficiency of genome editing as determined by next-generation sequencing correlates
321 with phenotype in b692 edited embryos. In high-rescued embryos, we find that 17% of
322 reads (106428 edited/641281 total) harbor an edited codon restoring Ser215 to Ile,
323 consistent with template integration. Analysis of aligned reads at exon 7 reveals the
324 uniform presence of barcoded nucleotides from the HDR template across the sgRNA
325 target site (Figure 3A). Phenotypic rescue in medium and low categories revealed
326 molecular efficiency of approximately 3% (14810/575344 and 17566/622068 reads,
327 respectively). Injected embryos with no phenotypic evidence of HDR had molecular

328 efficiency of <0.3%. Alignment of reads demonstrates a mutually exclusive pattern of
329 either HDR with template integration or indels at the sgRNA site (Figure 3A), consistent
330 with highly efficient dsDNA cleavage. We analyzed the molecular efficiency across all
331 phenotypes and plotted the fraction of reads harboring barcoded nucleotides from the
332 HDR template (Figure 3B-E). These data confirm the sensitivity of the b692-HDR assay
333 to read out the molecular efficiency of HDR in vivo.
334
335 **Genome editing using synthetic reagents leads to efficient fluorophore knock-in**
336 **and germline transmission**
337
338 To determine the feasibility of using synthetic reagents to knock-in a fluorophore by
339 HDR, we targeted *tyrp1b*, a melanocyte-specific gene. Using albino embryos
340 (pigmentless due to a null mutation in *slc45a2*) we performed microinjection of rCas9
341 with a synthetic sgRNA and a synthetic linear dsDNA template designed to knock EGFP
342 in frame with the terminal *tyrp1b* exon (Figure 4A). We identified 7/153 (5%) embryos
343 with EGFP-positive melanocytes at 48hpf (Figure 4B). Allele-specific PCR was
344 performed from injected embryos with EGFP-positive melanocytes (Figure 4C). Sanger
345 sequencing revealed the presence of multiple barcoded nucleotides encoded by the
346 HDR template, consistent with template integration (Figures 4D). Confocal imaging
347 revealed the presence of an EGFP-positive melanocyte with characteristic stellate
348 morphology (Figure 4D).
349
350 To determine the generalizability of this approach across multiple loci, we targeted
351 *h3f3a*, one of several genes encoding histone H3.3. We designed a linear dsDNA
352 template to knock EGFP in frame with *h3f3a*, creating a C-terminal fusion (Figure 4F).
353 We microinjected rCas9 with a synthetic sgRNA targeting *h3f3a* and a synthetic dsDNA
354 template into wild type embryos. We identified 12/152 (8%) embryos with EGFP-positive
355 cells at 48hpf (Figure 4G). Allele-specific PCR and Sanger sequencing performed on
356 EGFP positive embryos revealed precise template integration (Figure 4H,I). Confocal
357 imaging revealed the presence of cells with a nuclear EGFP-positive signal

358 characteristic of chromatin (Figure 6J). We raised mosaic F_0 embryos to adulthood and
359 assayed the rate of germline transmission. Of the 14 adult fish that mated, 2 (14%)
360 produced EGFP+ F_1 embryos (Figure 4K,L). Taken together, these data demonstrate
361 the ability of synthetic sgRNAs and dsDNA templates to knock-in allele-specific
362 fluorophores at several genomic loci and to transmit these edited alleles through the
363 germline.
364
365 To expand the applications of genome editing using synthetic DNA templates, we
366 targeted the liver-specific gene *fabp10a* using a linear dsDNA template that knocks in
367 mScarlet and bacterial nitroreductase (*ntr*) to facilitate hepatocyte ablation studies
368 (Figure 5A). The zebrafish liver is capable of regeneration after injury {Cox, 2015 #40},
369 and expression of *ntr* has been used in combination with metronidazole (Mtz) to cause
370 cellular injury {Curado, 2008 #41}. We injected embryos with rCas9, sgRNA targeting
371 *fabp10a*, and the HDR template and raised mScarlet+ F_0 embryos to adulthood. Of
372 adult fish that mated, 2/8 (25%) produced mScarlet+ F_1 embryos. We characterized the
373 recovered *fabp10a* allele in F_1 animals using allele-specific PCR and confirmed
374 integration of the template in mScarlet+ embryos (Figure 5B). Molecular analysis
375 indicated that the 5' end of the HDR template resulted in an in-frame fusion between
376 exon 4 and mScarlet. At the 3' end of the recovered allele, we identified a fragment of
377 exon 4 distal to the sgRNA recognition sequence, likely resulting from ligation to the
378 template. We treated transgenic F_1 embryos with Mtz to examine whether an fab10a-ntr
379 fusion was functional and could leave to liver-specific cytotoxicity. Exposing fabp10a-
380 mScarlet-NTR larvae to Mtz from 96–120 hpf resulted in a dramatic reduction in the
381 mScarlet fluorescent signal, signifying hepatocyte ablation without obvious damage to
382 other tissues (Figure 5C,D). Remnants of the ablated hepatocytes were observed
383 circulating in the vasculature. After a recovery period of 48 hours in the absence of Mtz,
384 mScarlet signal was observed in the liver of the Mtz-treated larvae, consistent with liver
385 regeneration (Figure 5E,F).
386
387 **DISCUSSION**

388

389 Here we describe the development and application of genome editing in zebrafish using
390 synthetic reagents. We demonstrate that the combined use of synthetic sgRNAs with
391 rCas9 protein leads to highly efficient indels. The improved efficiency of commercial
392 sgRNAs may result from chemical modifications that protect sgRNAs from degradation.
393 In order to optimize the efficiency of homology-directed repair we developed a genetic
394 assay using *mitfa*(b692) mutant zebrafish. Our data demonstrate that the b692-HDR
395 assay permits correlation between phenotype and HDR allele conversion (genotype).
396 Using this assay, we systematically tested multiple template designs to determine which
397 parameters are optimal for efficient knock-in by HDR. We find that the optimal template
398 is a linear, dsDNA template with an asymmetric sgRNA site. Using these design
399 principles, we knock-in fluorophores at *tyrp1b*, *h3f3a* and *fabp10a*; we achieved
400 germline transmission rates of 14–25% at two loci. At *fabp10a* the HDR template
401 included an *ntr* cassette to facilitate lineage ablation studies, and application of
402 metronidazole resulted in hepatocyte ablation in transgenic F_1 larvae. These germline
403 transmission rates are among the highest reported for knock-in of gene cassettes in
404 zebrafish, and this is the first report of CRISPR-mediated *ntr* knock-in and lineage
405 ablation.

406

407 A total synthetic approach has the unique advantage that sgRNA and HDR templates
408 can be designed in silico and commercially manufactured in a short time frame. Design
409 and precision genome editing with a synthetic dsDNA template can be performed within
410 2–3 weeks. The use of synthetic reagents may reduce experimental variability between
411 labs. The use of sgRNAs produced by commercial solid phase synthesis raises the
412 possibility of incorporating degeneracy in the sgRNA sequence to permit a single
413 sgRNA to target multiple related genes. The synthesis of linear dsDNA templates may
414 allow investigators to rapidly test sequence requirements for HDR. We unexpectedly
415 found significant differences in HDR efficiency between templates with minor design
416 differences. These observations suggest that empiric optimization of donor templates
417 may be required to achieve knock-in at some loci. As new recombinant Cas9 proteins

418 become available, the ability to perform base editing and other enzyme modifications
419 may be possible. Finally, the b692-HDR assay may be used as a screening platform to
420 identify chemical and genetic modifiers of HDR efficiency to make further improvements
421 in efficiency.
422
423 The use of CRISPR/Cas9 to generate loss of function mutations in zebrafish and other
424 model organisms makes it a uniquely valuable resource for forward genetics. To our
425 knowledge, this is the first study to develop a genetic assay for HDR in zebrafish and to
426 optimize HDR templates. Our studies offer insight into the relative efficiency of HDR and
427 provide investigators with a workflow for generating knock-in alleles. Our approach to
428 genome editing should allow investigators to pursue a broad range of in vivo
429 applications, including tissue-restricted lineage ablation, fluorophore and epitope knock-
430 in, and generation of conditional alleles. Future improvements in HDR efficiency may
431 occur with new variations in Cas9 protein and molecular and chemical tools to further
432 enhance the efficiency of homology directed repair.
433
434
435 **ACKNOWLEDGMENT**
436
437 We are grateful to members of the Houvras laboratory for critical discussion and
438 manuscript review. We thank the Weill Cornell Genomics Resources Core Facility for
439 next generation sequencing.
440
441 **FUNDING**
442
443 This work was supported by the Department of Surgery, Weill Cornell Medical College
444 (YH); National Institutes of Health/National Cancer Institute pre-doctoral fellowship
445 F31CA192813 (SED); National Institutes of Health/National Cancer Institute pre-
446 doctoral fellowship F31CA213997 (RM); the Medical Scientist Training Program of
447 General Medical Sciences of the NIH (T32GM007739) to the Weill

Cornell/Rockefeller/Sloan-Kettering Tri-Institutional MD-PhD Program (RM); the National Center for Advancing Translational Sciences of the NIH (TL1-TR000459) (CKG); the American Liver Foundation (PJW); the National Institutes of Health post-doctoral fellowship F32AA025271 (PJW); the National Institutes of Health R01DK090311 (WG), R01DK105198 (WG), R24OD017870 (WG), and the Claudia Adams Barr Program in Innovative Basic Cancer Research (WG). Wolfram Goessling is a Pew Scholar in the Biomedical Sciences. The content is solely the responsibility of the authors and does not necessarily represent the official views of the National Institutes of Health.

CONFLICT OF INTEREST

The authors declare no competing financial interests.

REFERENCES

1. Jao,L.-E., Wente,S.R. and Chen,W. (2013) Efficient multiplex biallelic zebrafish genome editing using a CRISPR nuclease system. *Proc. Natl. Acad. Sci. U. S. A.*, **110**, 13904–9.
2. Shah,A.N., Davey,C.F., Whitebirch,A.C., Miller,A.C. and Moens,C.B. (2015) Rapid reverse genetic screening using CRISPR in zebrafish. *Nat. Methods*, **12**, 535–540.
3. Auer,T.O., Duroure,K., Cian,A. De, Concordet,J. and Bene,F. Del (2014) Highly efficient CRISPR / Cas9-mediated knock-in in zebrafish by homology-independent DNA repair. *Genome Res.*, **24**, 142–153.
4. Irion,U., Krauss,J. and Nusslein-Volhard,C. (2014) Precise and efficient genome editing in zebrafish using the CRISPR/Cas9 system. *Development*, 10.1242/dev.115584.
5. Hoshijima,K., Jurynec,M.J. and Grunwald,D.J. (2016) Precise Editing of the Zebrafish Genome Made Simple and Efficient. *Dev. Cell*, **36**, 654–667.
6. Hwang,W.Y., Fu,Y., Reyon,D., Maeder,M.L., Kaini,P., Sander,J.D., Joung,J.K., Peterson,R.T. and Yeh,J.R.J. (2013) Heritable and Precise Zebrafish Genome Editing Using a CRISPR-Cas System. *PLoS One*, **8**, 1–9.
7. Kimura,Y., Hisano,Y., Kawahara,A. and Higashijima,S.I. (2014) Efficient generation of knock-in transgenic zebrafish carrying reporter/driver genes by CRISPR/Cas9-mediated genome engineering. *Sci. Rep.*, **4**, 1–7.
8. Hendel,A., Bak,R.O., Clark,J.T., Kennedy,A.B., Ryan,D.E., Roy,S., Steinfeld,I., Lunstad,B.D., Kaiser,R.J., Wilkens,A.B., *et al.* (2015) Chemically modified guide RNAs enhance CRISPR-Cas genome editing in human primary cells. *Nat. Biotechnol.*, **33**, 985–989.
9. Rahdar,M., McMahon,M.A., Prakash,T.P., Swayze,E.E., Bennett,C.F. and Cleveland,D.W. (2015) Synthetic CRISPR RNA-Cas9-guided genome editing in human cells. *Proc. Natl. Acad. Sci.*, **112**, E7110-7117.

10. Chari,R., Mali,P., Moosburner,M. and Church,G.M. (2015) Unraveling CRISPR-Cas9 genome engineering parameters via a library-on-library approach. *Nat. Methods*, **12**, 1–7.
11. Chari,R., Yeo,N.C., Chavez,A. and Church,G.M. (2017) SgRNA Scorer 2.0: A Species-Independent Model to Predict CRISPR/Cas9 Activity. *ACS Synth. Biol.*, **6**, 902–904.
12. Perez,A.R., Pritykin,Y., Vidigal,J.A., Chhangawala,S., Zamparo,L., Leslie,C.S. and Ventura,A. (2017) GuideScan software for improved single and paired CRISPR guide RNA design. *Nat. Biotechnol.*, **35**, 347–349.
13. Varshney,G.K., Zhang,S., Pei,W., Adomako-Ankomah,A., Fohtung,J., Schaffer,K., Carrington,B., Maskeri,A., Slevin,C., Wolfsberg,T., *et al.* (2016) CRISPRz: A database of zebrafish validated sgRNAs. *Nucleic Acids Res.*, **44**, D822–D826.
14. Lindsay,H., Burger,A., Biyong,B., Felker,A., Hess,C., Zaugg,J., Chiavacci,E., Anders,C., Jinek,M., Mosimann,C., *et al.* (2016) CrispRVariants charts the mutation spectrum of genome engineering experiments. *Nat. Biotechnol.*, **34**, 701–702.
15. Draper,B.W. and Moens,C.B. (2009) A High-Throughput Method For Zebrafish Sperm Cryopreservation and In Vitro Fertilization. *J. Vis. Exp.*, 10.3791/1395.
16. Meeker,N.D., Hutchinson,S.A., Ho,L. and Trede,N.S. (2007) Method for isolation of PCR-ready genomic DNA from zebrafish tissues. *Biotechniques*, **43**, 610–614.
17. Carrington,B., Varshney,G.K., Burgess,S.M. and Sood,R. (2015) CRISPR-STAT: An easy and reliable PCR-based method to evaluate target-specific sgRNA activity. *Nucleic Acids Res.*, **43**, 1–8.
18. Holleley,C.E. and Geerts,P.G. (2009) Multiplex Manager 1.0: A cross-platform computer program that plans and optimizes multiplex PCR. *Biotechniques*, **46**, 511–517.
19. Dobin,A., Davis,C.A., Schlesinger,F., Drenkow,J., Zaleski,C., Jha,S., Batut,P., Chaisson,M. and Gingeras,T.R. (2013) STAR: Ultrafast universal RNA-seq aligner. *Bioinformatics*, **29**, 15–21.
20. Thorvaldsdóttir,H., Robinson,J.T. and Mesirov,J.P. (2013) Integrative Genomics Viewer (IGV): High-performance genomics data visualization and exploration. *Brief. Bioinform.*, **14**, 178–192.
21. Robinson,J.T., Thorvaldsdottir,H., Winckler,W., Guttman,M., Lander,E.S., Getz,G. and Mesirov,J.P. (2011) Integrative Genomics Viewer. *Nat. Biotechnol.*, **29**, 24–26.
22. Sheets,L., Ransom,D.G., Mellgren,E.M., Johnson,S.L. and Schnapp,B.J. (2007) Zebrafish Melanophilin Facilitates Melanosome Dispersion by Regulating Dynein. *Curr. Biol.*, **17**, 1721–1734.
23. Lister,J., Robertson,C., Lepage,T., Johnson,S. and Raible,D. (1999) Nacre Encodes a Zebrafish Microphthalmia-Related Protein That Regulates Neural-Crest-Derived Pigment Cell Fate. *Development*, **126**, 3757–3767.
24. Lister,J.A., Close,J. and Raible,D.W. (2001) Duplicate mitf genes in zebrafish: Complementary expression and conservation of melanogenic potential. *Dev. Biol.*, **237**, 333–344.
25. Richardson,C.D., Ray,G.J., DeWitt,M.A., Curie,G.L. and Corn,J.E. (2016)

532 Enhancing homology-directed genome editing by catalytically active and inactive
533 CRISPR-Cas9 using asymmetric donor DNA. *Nat. Biotechnol.*, **34**, 339–344.
534 26. Varshney,G.K., Pei,W., Lafave,M.C., Idol,J., Xu,L., Gallardo,V., Carrington,B.,
535 Bishop,K., Jones,M., Li,M., *et al.* (2015) High-throughput gene targeting and
536 phenotyping in zebrafish using CRISPR / Cas9. *Genome Res.*, **25**, 1–13.
537 27. Quadros,R.M., Miura,H., Harms,D.W., Akatsuka,H., Sato,T., Aida,T., Redder,R.,
538 Richardson,G.P., Inagaki,Y., Sakai,D., *et al.* (2017) Easi-CRISPR: A robust method
539 for one-step generation of mice carrying conditional and insertion alleles using long
540 ssDNA donors and CRISPR ribonucleoproteins. *Genome Biol.*, **18**, 1–15.
541 28. Anantha,R.W., Simhadri,S., Foo,T.K., Miao,S., Liu,J., Shen,Z., Ganesan,S. and
542 Xia,B. (2017) Functional and mutational landscapes of BRCA1 for homology-
543 directed repair and therapy resistance. *Elife*, **6**, 1–21.
544 29. Westerfield M. 2007. The Zebrafish Book a Guide for the Laboratory Use of
545 Zebrafish (Danio Rerio). 5th Edition. Eugene: University of Oregon Press.
546

547 **FIGURE LEGENDS**
548
549 **Figure 1.** Synthetic sgRNAs outperform laboratory synthesized *in vitro* transcribed
550 sgRNAs**.** (**A**) Dose-response comparison of editing in embryos injected with rCas9 and
551 either an *in vitro* synthesized or synthetic sgRNA targeting *tyr*. Embryos were scored for
552 melanocyte dropout at 48hpf and binned into 4 categories. The percentage of embryos
553 in each condition is plotted. At the 1000pg sgRNA/2000pg rCas9 dose, there is a
554 statistically significant increase in the editing observed with the synthetic sgRNA
555 (p=<0.001, Chi-square). (**B**) Light microscopic images of representative embryos in
556 each category. (**C)** CrisprVariants {Lindsay, 2016 #18} plot of indels in clones isolated
557 from embryos injected with either synthetic or *in vitro* transcribed sgRNAs. 10/10 clones
558 isolated from individual embryos injected with synthetic from sgRNAs contained indels
559 and 7/10 clones isolated from embryos injected with IVT sgRNAs contained indels.
560
561 **Figure 2.** A genetic assay for optimizing homology-directed repair using b692 mutant
562 zebrafish. (**A**) *mitfa*(b692) embryos uninjected (top), injected with rCas9, 951bp DNA
563 template, and non-targeting sgRNA (middle) or *mitfa* sgRNA (bottom). All embryos
564 shown at 48hpf. (**B**) Schematic depicting *mitfa* gene structure and location of the
565 mutation in exon 7 in b692 mutants. The sgRNA location is indicated. Primers used for
566 allele-specific PCR are displayed as orange arrows. A linear 951bp dsDNA template
567 encodes a wild-type Ile codon at position 215 and additional nucleotide changes to
568 prevent re-cleavage at the sgRNA recognition site (red). (**C**) Allele-specific PCR was
569 performed on rescued embryos after microinjection with 951bp template and compared
570 with uninjected embryos. (**D**) Sanger sequencing results of allele-specific PCR products
571 from a phenotypically rescued embryo. The sequence read spans the template-genome
572 junction and includes template specific barcoded nucleotides. (**E**) Chart depicting
573 attributes of DNA template (left), a description of the template (middle) and observed
574 rate of rescue in the b692-HDR assay (right).
575
576 **Figure 3.** Quantitative assessment of genome editing efficiency by next-generation
577 sequencing. (**A**) Alignment of next generation sequencing reads from b692 genome
578 edited embryos from the high rescue phenotype. Exon 7 of *mitfa* is displayed. The
579 sgRNA sequence is highlighted in yellow. b692 mutants have a T>G mutation leading to
580 an isoleucine to serine substitution at codon 215(*). The 951bp dsDNA template
581 restores the wild-type isoleucine codon (ATC) and encodes nine additional barcoded
582 nucleotides as indicated. Indels in sequencing reads are represented as gapped regions
583 in black. (**B-E**) The fraction of reads at each barcoded nucleotide in the HDR template is
584 plotted for each phenotype category.
585
586 **Figure 4.** Genome editing leads to precise fluorophore knock-in. (**A**) Schematic
587 depicting *tyrp1b* locus. A linear, dsDNA template designed to lead to an in-frame EGFP
588 knock-in is shown. (**B**) albino(b4) embryo injected with rCas9, *tyrp1b* synthetic sgRNA,
589 and dsDNA template is photographed with light (top panel) or fluorescence (bottom
590 panel) microscopy at 48hpf. (**C**) Allele-specific PCR was performed on uninjected or

591 HDR edited/GFP+ embryos at 48hpf. Only HDR-edited/EGFP-positive embryos had a
592 PCR amplicon. (**D**) Sanger sequencing from allele-specific PCR to detect template
593 integration. The sequence was aligned to reference (top). Barcoded nucleotides at the
594 sgRNA binding site consistent with template integration were identified. A representative
595 chromatogram is shown. (**E**) Confocal imaging reveals the presence of stellate EGFP-
596 positive melanocytes. (**F**) Schematic depicting *h3f3a* locus. A linear, dsDNA template
597 designed to lead to an in-frame EGFP knock-in is shown. (**G**) Wild-type embryo injected
598 with rCas9, *h3f3a* sgRNA, and dsDNA template is photographed with light (top panel) or
599 fluorescence (bottom panel) microscopy (48hpf). (**H**) Allele-specific PCR was performed
600 on uninjected or HDR edited/GFP+ embryos at 48hpf. Only HDR-edited/EGFP-positive
601 embryos had a PCR amplicon. (**I**) Sanger sequencing was performed from allele-
602 specific PCR to detect template integration. The sequence was aligned to reference
603 (top). Barcoded nucleotides at the sgRNA binding site, consistent with template
604 integration were identified. A representative chromatogram is shown. (**J**) Confocal
605 imaging reveals the presence of an EGFP-positive nuclei. (K-L) Immunofluorescent
606 images of F1 progeny showing transmission of EGFP from h3f3a-EGFP founder.
607
608 **Figure 5.** Knock-in of a synthetic dsDNA template encoding a fluorophore and bacterial
609 nitroreductase enables tissue-specific ablation. (**A**) Schematic outlining HDR template
610 design at the *fabp10a* locus. A 2.0kB template was designed to insert mScarlet-NTR as
611 a C-terminal fusion to the *fabp10a* gene, which has hepatocyte-specific expression. The
612 recovered allele from F_1 progeny confirms integration of mScarlet after the last coding
613 exon of *fabp10a*. **(B)** Allele-specific PCR was performed to confirm integration of the
614 template in mScarlet+ (mS+) embryos. (**C-F**) Mtz exposure induced hepatocyte injury in
615 fabp10a-mScarlet-NTR larvae. **(C)** Confocal imaging revealed loss of fluorescence in
616 the liver (outlined) of Mtz-treated but not DMSO-treated larvae. Remnants of ablated
617 hepatocytes were found distributed throughout the vasculature (arrowhead). **(D)**
618 Confocal imaging of liver in DMSO- and Mtz-treated larvae after injury. (**E**) At 48 hours
619 post injury (hpi), mScarlet signal was observed in the liver (outlined) of the Mtz-treated
620 larvae, demonstrating liver regeneration. **(F)** Confocal imaging of liver in DMSO and Mtz
621 treated larvae at 48 hpi. Scale bars are 200 μm (C,E) and 30 μm (D,F).
622
623 **Supplementary Figure 1.** Synthetic sgRNAs outperform *in vitro* synthesized sgRNA in
624 targeting *slc25a2* (golden) and *slc45a2* (albino). (**A**) Comparison of Alt-R® synthetic
625 sgRNA preparation and *in vitro* synthesis of sgRNAs. Left, Alt-R® synthetic sgRNAs are
626 prepared by duplexing a gene specific crRNA with a common tracrRNA. Right, IVT
627 sgRNAs are transcribed from a DNA template using RNA polymerase and purified. Both
628 sgRNAs are used with rCas9 and microinjected into embryos at the one-cell stage. (**B**)
629 Light microscopic images of representative embryos in each phenotypic category. (**C**)
630 Dose-response comparison of editing in embryos injected with rCas9 and either an *in*
631 *vitro* synthesized or synthetic sgRNA targeting *slc25a2*. Embryos were scored for
632 melanocyte dropout at 48hpf and binned into 4 categories. The percentage of embryos
633 in each condition is plotted. (D) Embryos injected with either IVT or synthetic sgRNA
634 targeting slc45a2 (albino). Representative embryos are shown. IVT sgRNA was

635 ineffective in inducing a mutant phenotype. Synthetic sgRNA induced a mutant
636 phenotype in virtually all injected embryos. (E) A clonal analysis was performed and
637 analyzed using CrisprVariants. IVT injected embryos showed no evidence of indels
638 (0/10 clones) and a synthetic sgRNA induced indels in 10/10 clones.
639
640 **Supplementary Figure 2.** Synthetic sgRNAs produce highly penetrant phenotypes in
641 F_0 injected animals. Wild-type (AB) embryos were injected with rCas9 and synthetic
642 sgRNA targeting *mlpha*. Uninjected larval animals (top) have normal stripe pattern.
643 Juvenile zebrafish (7 weeks post fertilization) injected with rCas9 and a synthetic
644 sgRNA targeting *mlpha* show reduced pigmentation and phenocopies an established
645 mutant.
646
647 **Supplementary Figure 3.** Synthetic sgRNA pairs induce deletions in genomic DNA. (**A**)
648 Schematic of a 126kB genomic region targeted for deletions. Guide locations are
649 marked in purple, and primers used for PCR are displayed as orange arrows. Guide
650 pairs were co-injected into 1-cell stage embryos. (**B**) Table of predicted PCR product
651 size after inducing deletions and observed deletion frequency in individual F_0 injected
652 embryos. (**C-F**) PCR amplicons from individual embryos were subjected to Sanger
653 sequencing and analysis. The observed deletion size is indicated.
654
655 **Supplementary Figure 4.** Germline transmission of edited alleles is achieved using
656 synthetic sgRNAs. (**A**) Sperm samples were collected from a CRISPR-injected potential
657 F_0 founder and assayed using CRISPR-STAT fluorescence-based genotyping. (**B-F**)
658 CRISPR-STAT results for tail clips from representative F_1 progeny, each carrying one of
659 the distinct alleles with specific insertions and deletions (del3, del4, del7, del11), as well
660 as the wild-type (WT) allele, transmitted from the F_0 founder. The number of F_1 offspring
661 identified with each genotype is identified in the bottom right of each panel. Relative
662 fluorescence levels (y-axis) are shown against fragment size in base pairs (x-axis) for
663 each genotyping assay. PCR products consistent with predicted wild type amplicon size
664 are indicated by red asterisks. **(G)** Indels in F_0 sperm predict alleles transmitted to the
665 germline. Percentages shown are calculated as area under the curve for each peak in
666 the indicated tissue from the F_0 founder. The frequencies of each mutation in the F_1
667 progeny were calculated from a total of 17 siblings from a cross between the F_0 male
668 parent and a WT female.

669 **Supplementary Figure 5.** Comparison of melanocyte phenotypes in mitfa mutants after
670 targeting *mitfa* using CRISPR/Cas9. (**A**) *mitfa*(w2) embryos were injected with rCas9
671 and a specific sgRNA near the mutation site. Ten representative embryos at 24hpf are
672 shown. Melanocyte rescue occurs in a significant fraction of embryos. (**B**)
673 CrispRVariants plot from *mitfa*(w2) embryos injected with rCas9 and nacre gRNA. A
674 majority of embryos harbor indels. (**C**) mitfa(b692) embryos were injected with rCas9
675 and a synthetic sgRNA near the b692 mutation site (b692 sgRNA). Uninjected wild-type
676 (AB) embryos (top, left) have pigmented melanocytes at 48hpf. Wild-type embryos
677 injected with rCas9 and b692 sgRNA (bottom, left) have a highly penetrant loss of
678 melanocytes. Uninjected *mitfa*(b692) embryos (top, right) lack pigmentation because of

679 the b692 mutation. *mitfa*(b692) embryos injected with rCas9 and the b692 sgRNA
680 (bottom, right) have no evidence of melanocyte rescue.
681
682 **Supplementary Table 1.** sgRNA sequences. Sequences of sgRNA sequences are
683 noted with the PAM sequence in parentheses.
684
685 **Supplementary Table 2.** Primer sequences are listed for PCR reactions noted in the
686 text.
687
688

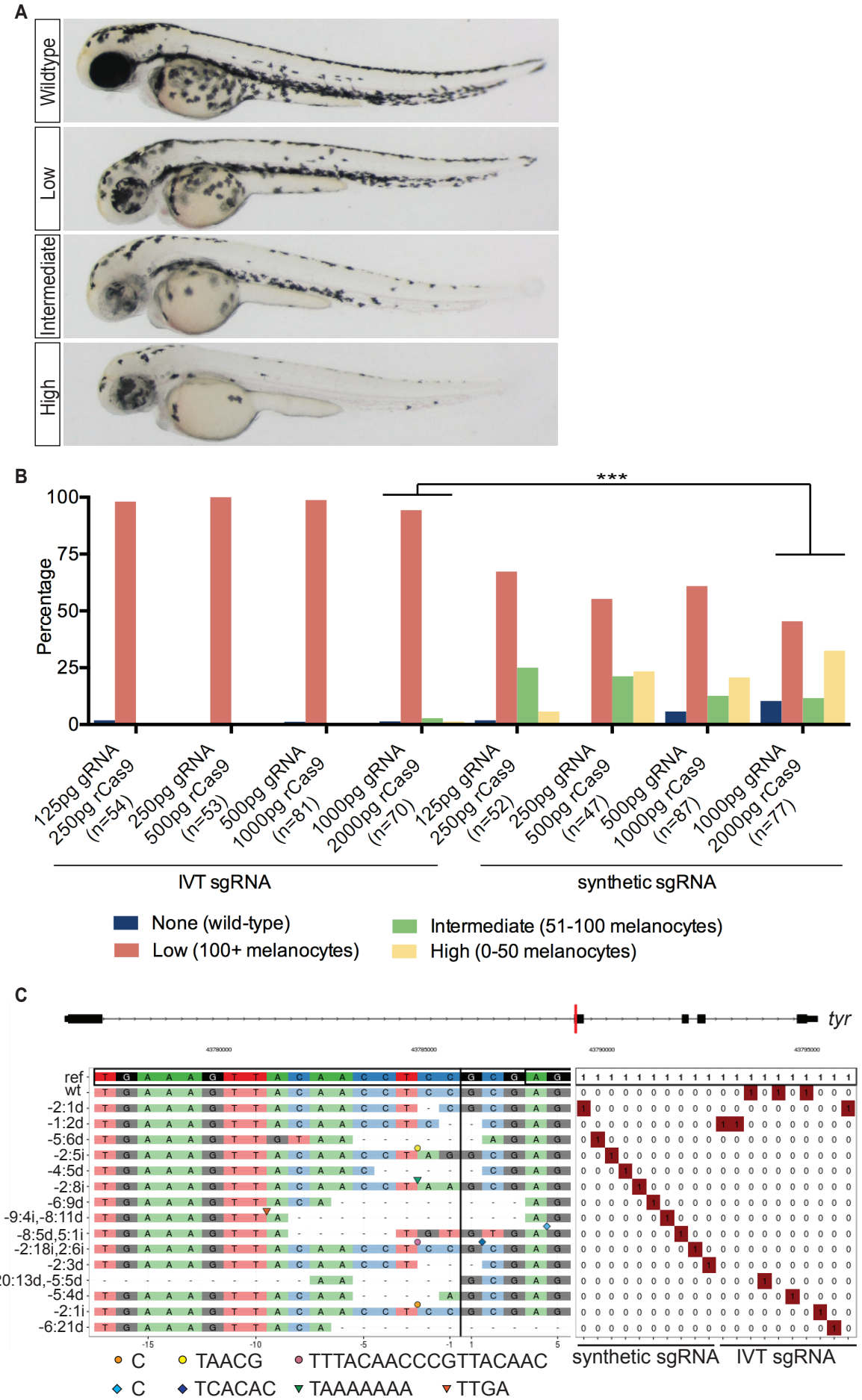
A
Wildtype
Low
Intermediate
High
B
***
Percentage
100
75
50
25
0
125pg gRNA 250pg rCas9 (n=54)
250pg gRNA 500pg rCas9 (n=53)
500pg gRNA 1000pg rCas9 (n=81)
1000pg gRNA 2000pg rCas9 (n=70)
125pg gRNA 250pg rCas9 (n=52)
250pg gRNA 500pg rCas9 (n=47)
500pg gRNA 1000pg rCas9 (n=87)
1000pg gRNA 2000pg rCas9 (n=77)
IVT sgRNA
synthetic sgRNA
None (wild-type)
Low (100+ melanocytes)
Intermediate (51-100 melanocytes)
High (0-50 melanocytes)
C
tyr
ref
wt
-2:1d
-1:2d
-5:6d
-2:5i
-4:5d
-2:8i
-6:9d
-9:4i,-8:11d
-8:5d,5:1i
-2:18i,2:6i
-2:3d
-20:13d,-5:5d
-5:4d
-2:1i
-6:21d
synthetic sgRNA
IVT sgRNA
C
TAACG
TTTACAACCCGTTACAAC
C
TCACAC
TAAAAAAA
TTGA

Figure 1

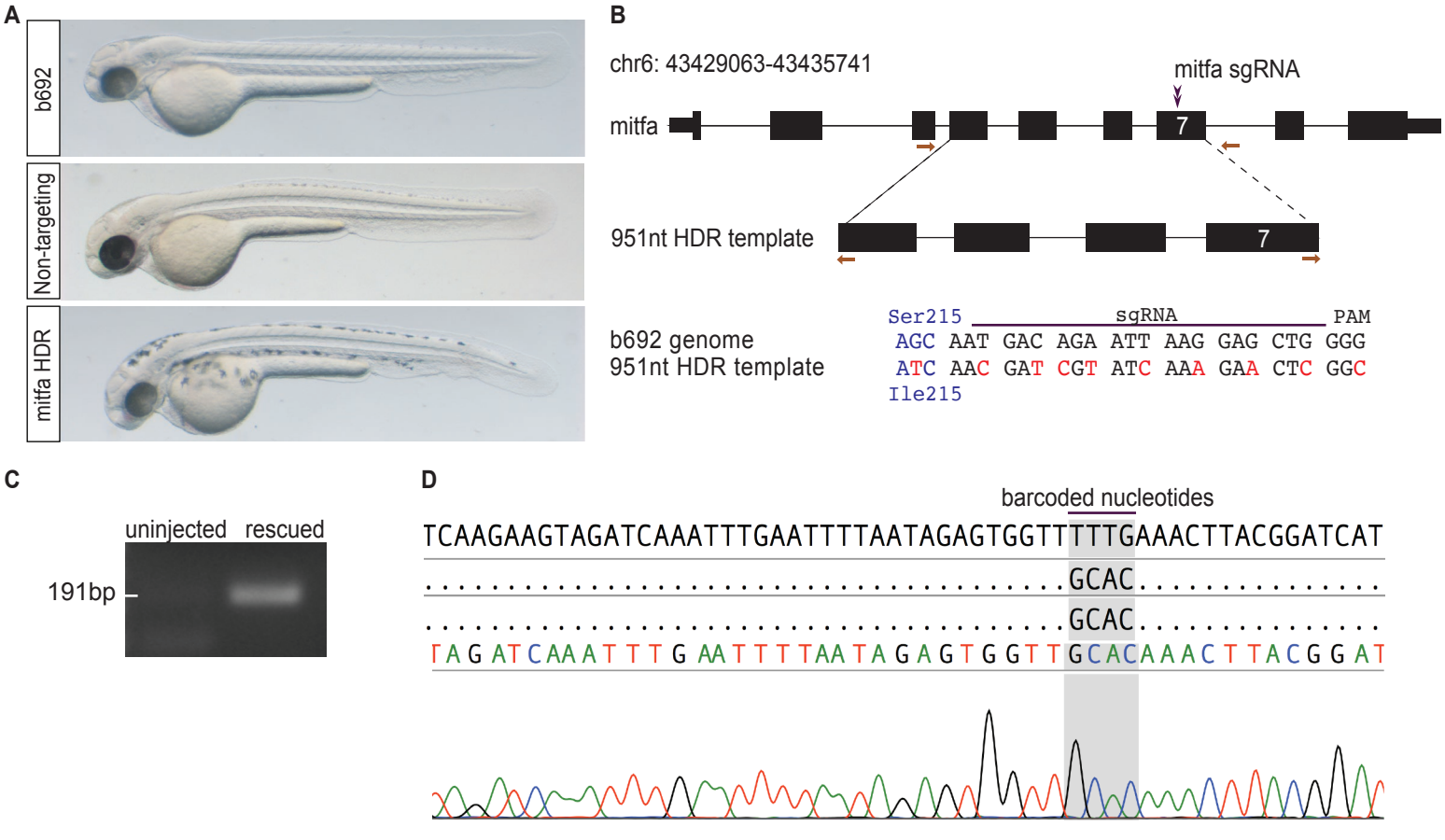

E

DNA template design	Strategy employed	HDR efficiency
	Asymmetric ds 951bp template	9%*
	Asymmetric ds 2000bp template	6%
	Asymmetric ds 951bp template slid 50bp	5%
	Asymmetric ds 951bp template slid 100bp	5%
	Asymmetric ds 318bp template	1%
	Asymmetric ds 951bp template with two guide sites	<1%
	5' asymmetric ds 951bp template	0%
	Symmetric ds 951bp template	0%
	Symmetric ds 2000bp template	0%
	Symmetric ds 76bp template	0%
	Symmetric ds 200bp template	0%
	Symmetric ss 200bp template	0%
	Symmetric ds 1214bp template with homologous flanking guide sites	0%
	Symmetric ds 896bp template with two guide sites	0%
	Symmetric ss 896bp template with two guide sites	0%
	Asymmetric ds 951bp template with nonhomologous flanking guide sites	0%
	Asymmetric ds 951bp template with flanking ISceI restriction enzyme sites	0%
	Asymmetric ds 951bp template with nickase-compatible guide sites	0%
	Asymmetric ds 951bp template in a vector	0%

Figure 2

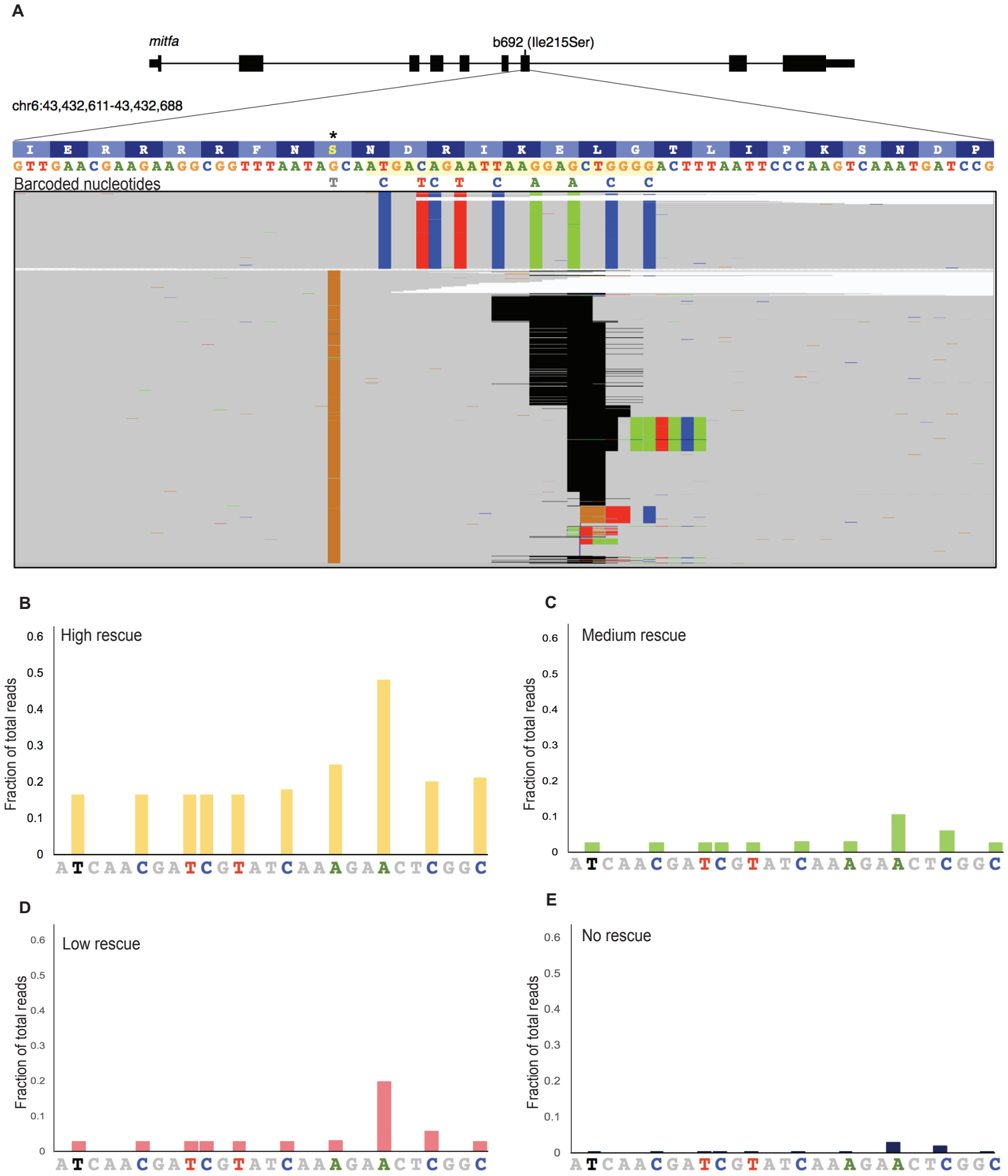
A
mitfa
b692 (Ile215Ser)
chr6:43,432,611-43,432,688
I E R R R R F N S N D R I K E L G T L I P K S N D P
GTTGAACGAAGAAGGCGGTTTAATAGCAATGACAGAATTAAGGAGCTGGGGACTTTAATTCCCAAGTCAAATGATCCG
Barcoded nucleotides
T C TC T C A A C C
B
High rescue
Fraction of total reads
0.6
0.5
0.4
0.3
0.2
0.1
0
ATCAACGATCGTATCAAAGAACTCGGC
C
Medium rescue
Fraction of total reads
ATCAACGATCGTATCAAAGAACTCGGC
D
Low rescue
Fraction of total reads
ATCAACGATCGTATCAAAGAACTCGGC
E
No rescue
Fraction of total reads
ATCAACGATCGTATCAAAGAACTCGGC

Figure 3

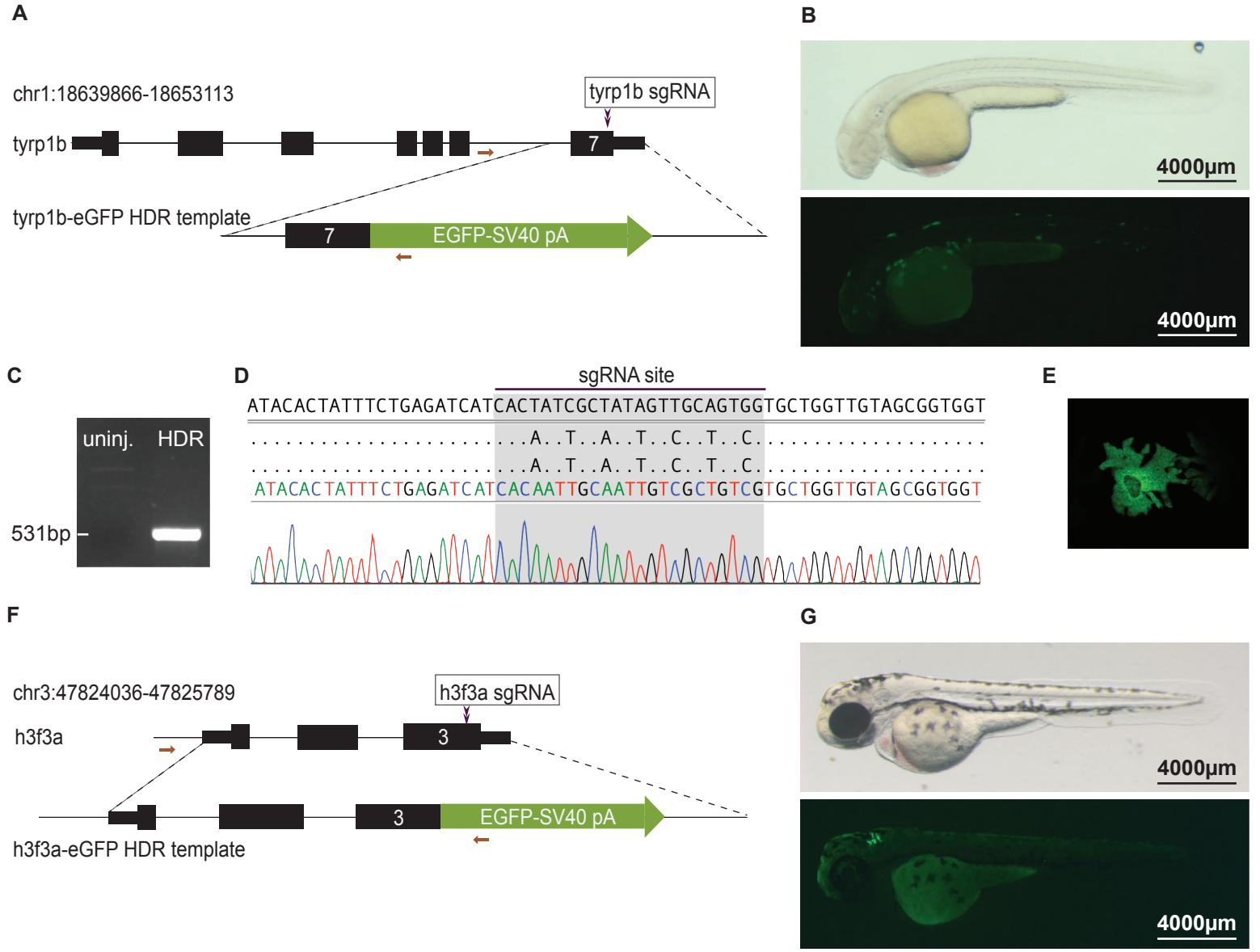
A
chr1:18639866-18653113
tyrp1b sgRNA
tyrp1b
7
tyrp1b-eGFP HDR template
7
EGFP-SV40 pA
B
4000μm
4000μm
C
uninj.
HDR
531bp
D
sgRNA site
ATACACTATTTCTGAGATCATCACTATCGCTATAGTTGCAGTGGTGCTGGTTGTAGCGGTGGT
ATACACTATTTCTGAGATCATCACAATTGCAATTGTCGCTGTCGTGCTGGTTGTAGCGGTGGT
E
F
chr3:47824036-47825789
h3f3a sgRNA
h3f3a
3
3
EGFP-SV40 pA
h3f3a-eGFP HDR template
G
4000μm
4000μm
H
uninj.
HDR
1001bp
I
sgRNA site
GCCATTCATGCCAAGAGAGTAACAATCATGCCCAAGGATATCCAGCTTGCAAGGCGAATCAGAGGAGAG
GCCATTCATGCCAAGAGAGTAACAATCATGCCCAAAGACATTCAACTCGCCAGACGAATCAGAGGAGAG
J
K
L

Figure 4

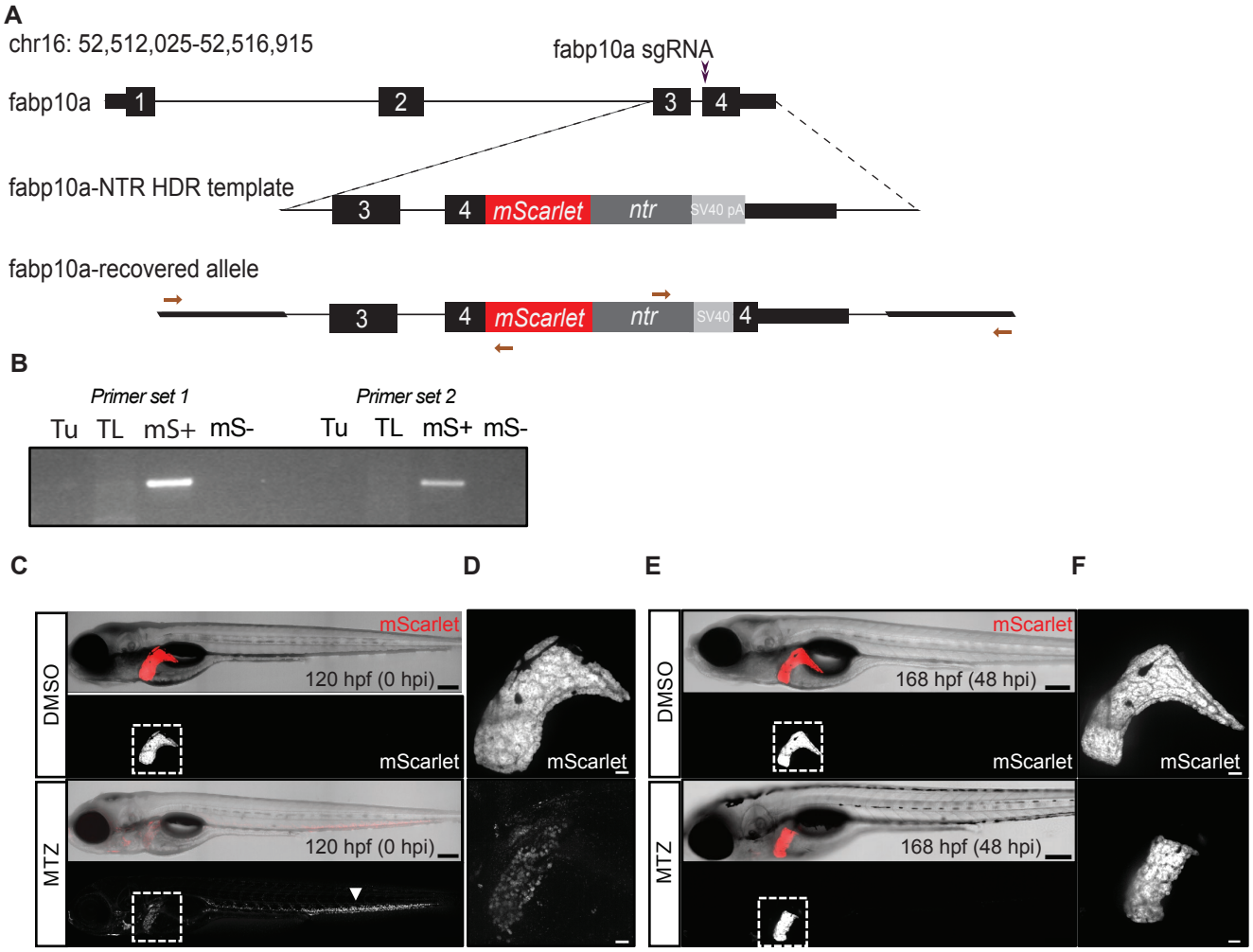
A
chr16: 52,512,025-52,516,915
fabp10a sgRNA
fabp10a
1
2
3
4
fabp10a-NTR HDR template
3
4
mScarlet
ntr
SV40 pA
fabp10a-recovered allele
3
4
mScarlet
ntr
SV40
4
B
Primer set 1
Tu TL mS+ mS-
Primer set 2
Tu TL mS+ mS-
C
D
E
F
DMSO
MTZ
mScarlet
120 hpf (0 hpi)
168 hpf (48 hpi)

Figure 5

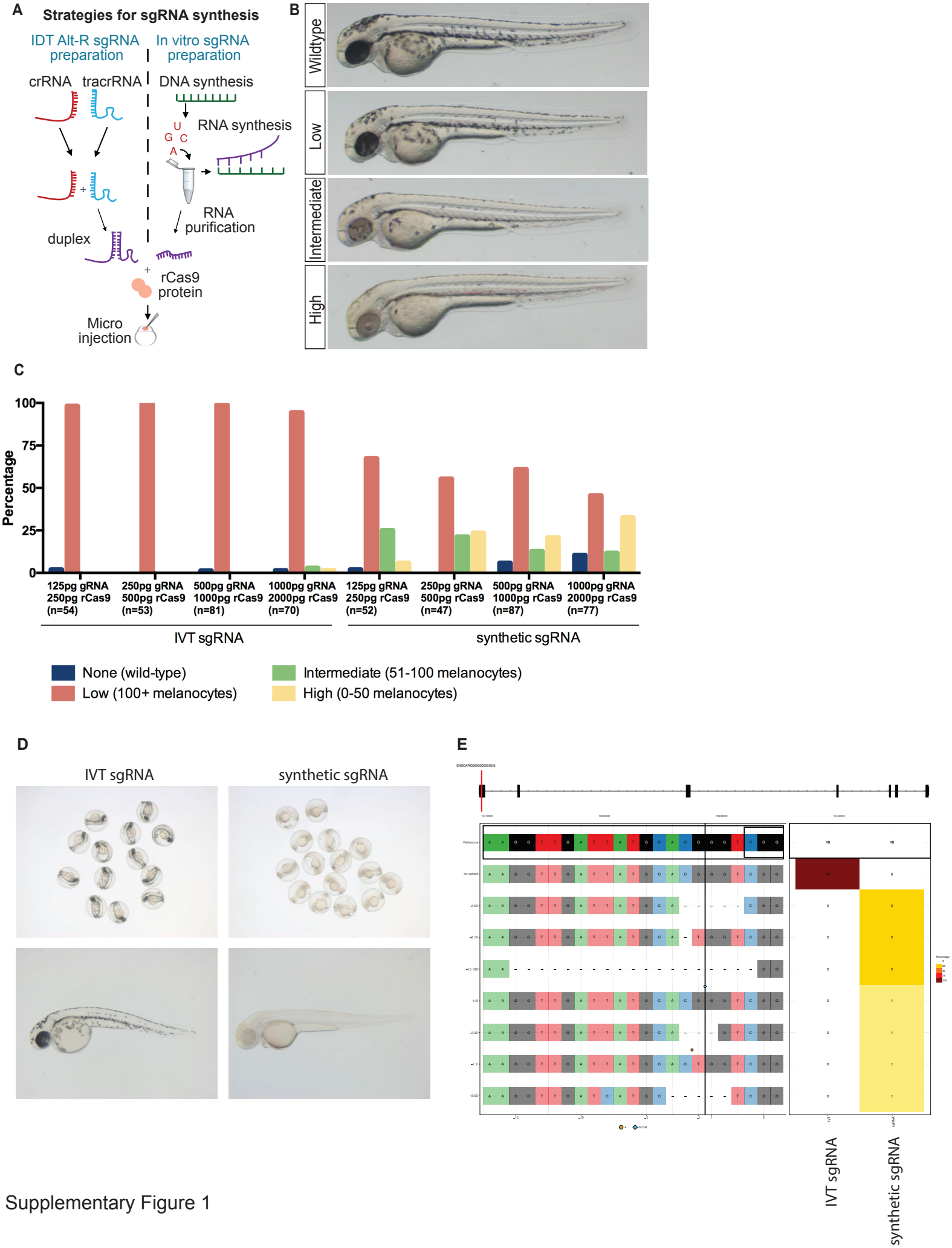

Supplementary Figure 1

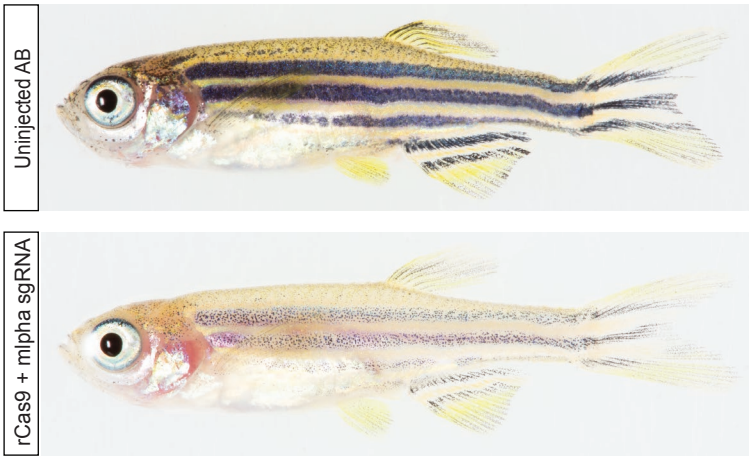

Supplementary Figure 2

A

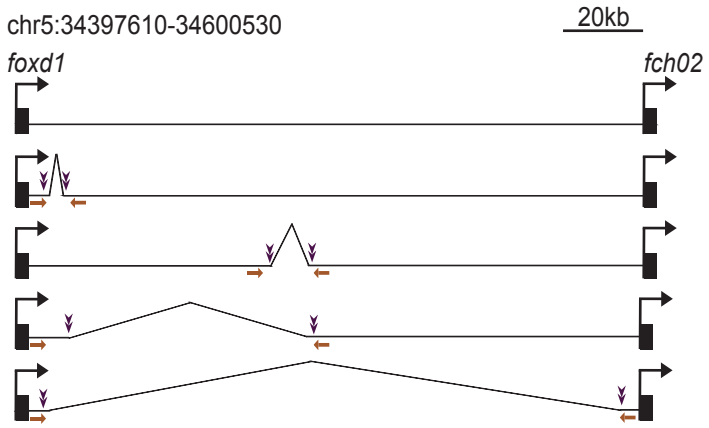

B

sgRNAs	Predicted deletion size	Observed deletion frequency
sgRNA1+2	0.45kb	5/10 (50%)
sgRNA3+4	4.3kb	7/24 (29%)
sgRNA2+4	52kb	3/8 (38%)
sgRNA1+5	124kb	2/23 (9%)

C

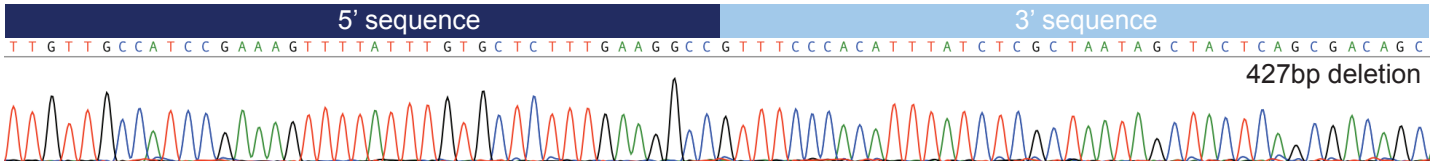

D

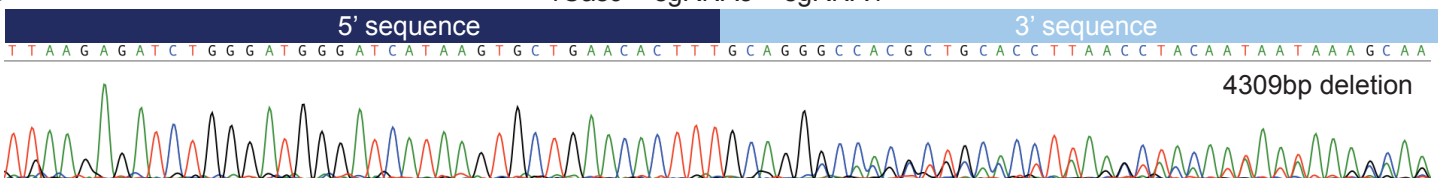

E

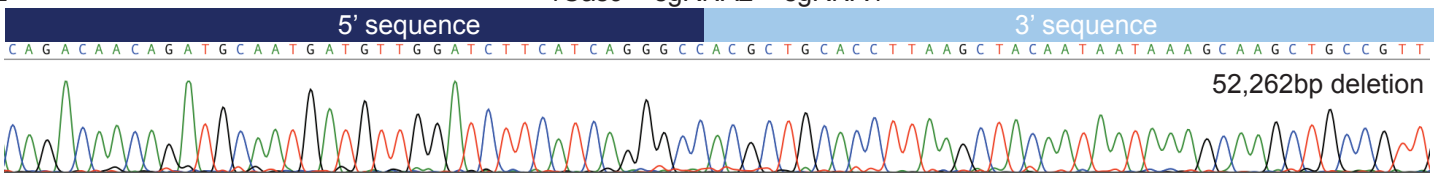

F

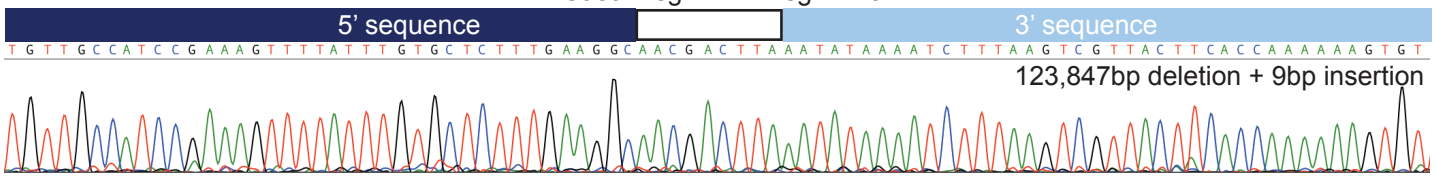

Supplementary Figure 3

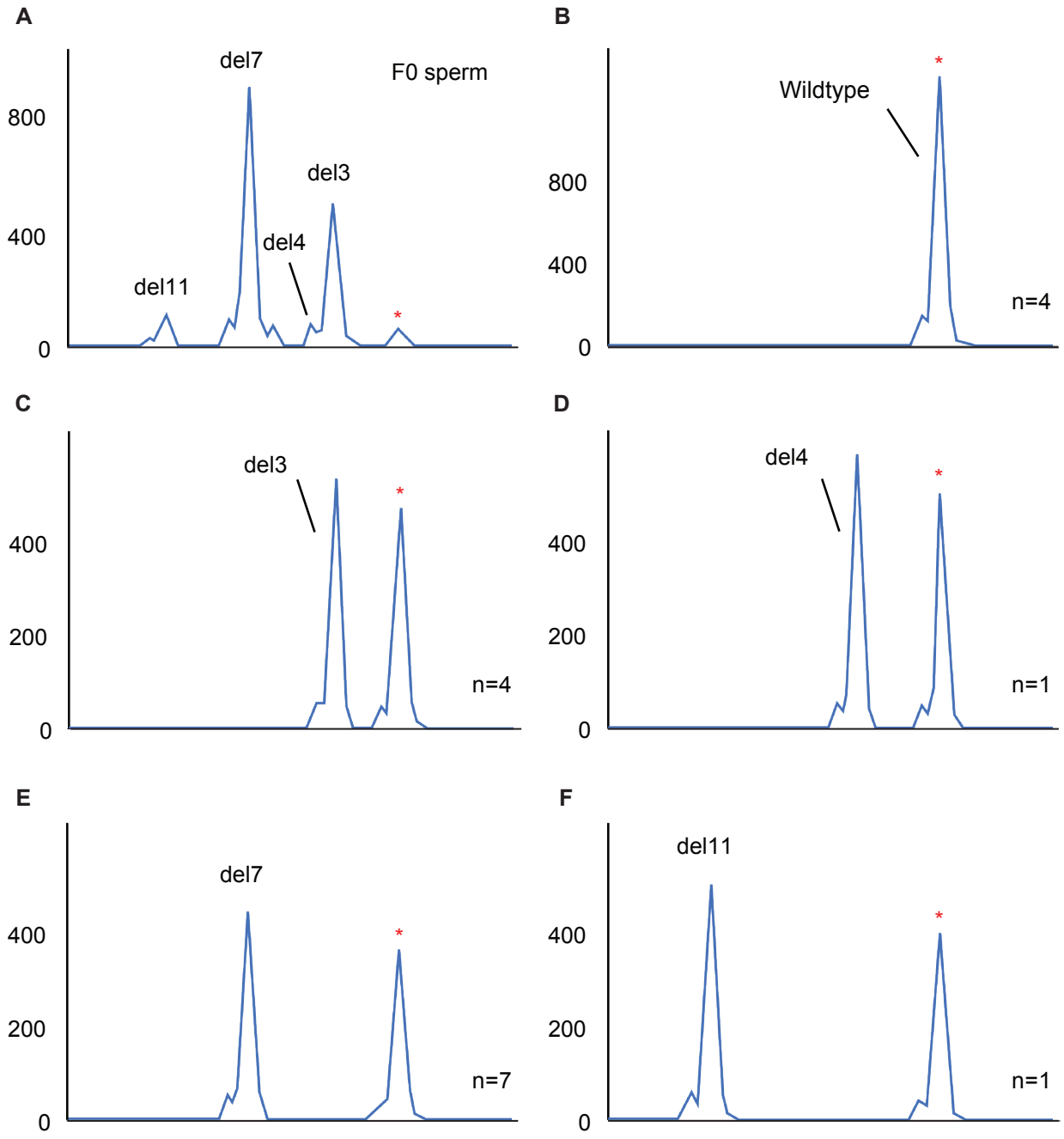

G

	F0 Sperm	F1 Progeny
del11	7.4%	5.9%
del7	58.9%	41.2%
del4	<5%	5.9%
del3	33.7%	23.5%
WT	<5%	23.5%
Total	100.0%	100.0%

Supplementary Figure 4

A

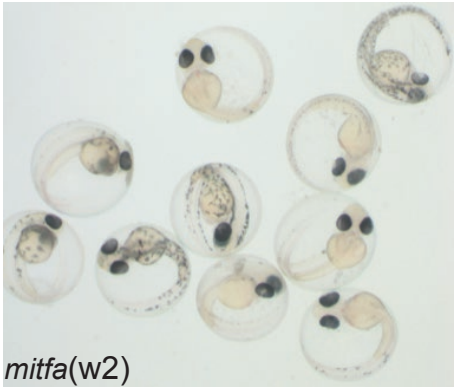

B

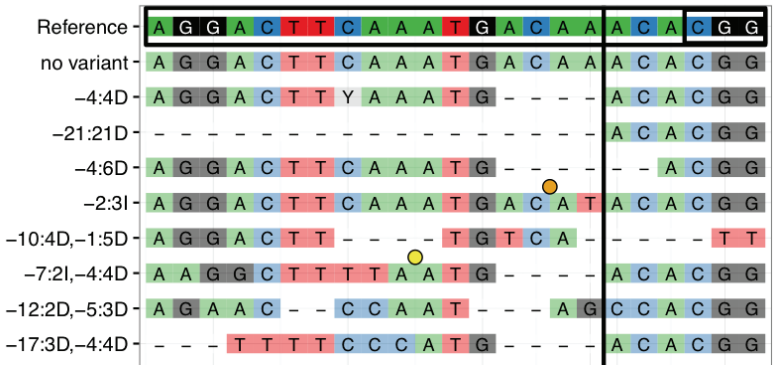

C

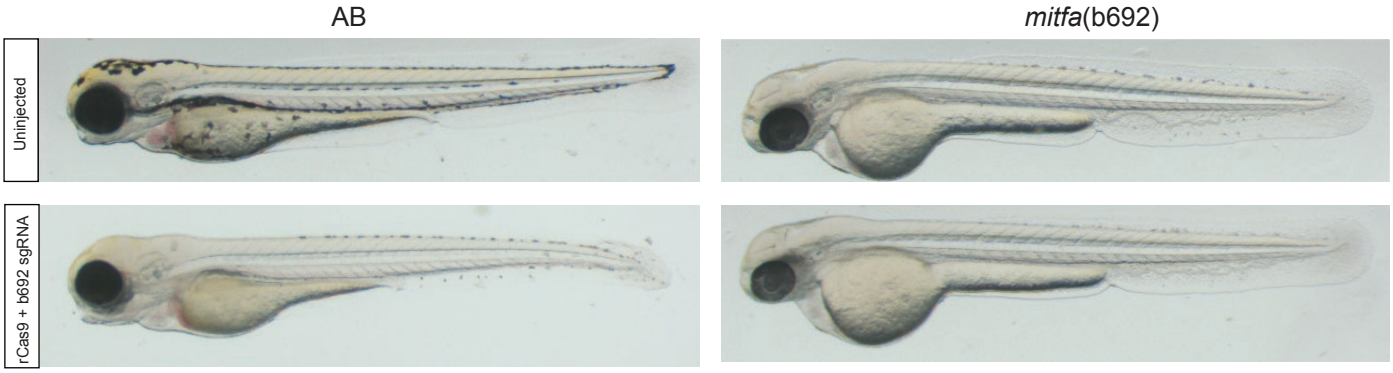

Supplementary Figure 5

Supplementary Table 1

sgRNA name	**sgRNA Sequence**
tyr	TGAAAGTTACAACCTCCGCG(AGG)
slc24a5 (golden)	GGTCTCTCGCAGGATGTTGC(TGG)
mitfa(w2)	AGGACTTCAAATGACAAACA(CGG)
mitfa(b692)	ATGACAGAATTAAGGAGCTG(GGG)
tyrp1b	CACTATCGCTATAGTTGCAG(TGG)
mlpha	AATGACCTCCCACACATGCT(TGG)
h3f3a	CAAGGATATCCAGCTTGCA(AGG)
non-targeting	TGCTGATGTCTTGGTTGAAT(TGG)
deletion_1	TGTGCTCTTTGAAGGCCATG(AGG)
deletion_2	TGTGGGAAACGGCATATATG(AGG)
deletion_3	AATCACCGAGAAATTGGAG(AGG)
deletion_4	CAGGCAGGATCAAAGAAGGC(AGG)
deletion_5	AATAGCTCATAAAGACGGTG(AGG)
slc6a15	GACTCCATCTCAGAGGGTGG(AGG)
fabp10a	GTGCAGACGCTGACAGTCGG(AGG)
slc45a2 (albino)	AAGGTTGATTATGCACGGGT(CGG)
wee1	TGATACCCCCCACACCCCAA(AGG)

Supplementary Table 2

Primer Name	Primer Sequence
tyr gRNA validation (F)	AATGTCGTTCACTCTGCTGTTG
tyr gRNA validation (R)	GTGACCGTGCTGTTGTACCTT
gol gRNA validation (F)	TGCTGGATGCCCTTGTCAAT
gol gRNA validation (R)	AAAGTAGGCGACACTGACGG
mitfa(w2) gRNA validation (F)	GTGGATTGAGGTTCCCTTCA
mitfa(w2) gRNA validation (R)	CGGATAATTCCCTTTTGACG
mitfa(b692) gRNA validation (F)	CAGAGCCCTGGCAAAAGAGA
mitfa(b692) gRNA validation (R)	TGTGTGCCTGCTGGGATTTA
mitfa_next_gen (F)	GCAGTTATTAATGATAATGTCTCG
mitfa_next_gen (R)	GGACTTAAGTAAATCAAGAAGTAGATC
tyrp1b gRNA validation (F)	ATGGAGCAGTTGAGGCTGTC
typ1b gRNA validation (R)	ATCCTCTGAGTAGCGCCTGA
mlpha gRNA validation (F)	CATTCAGTCTTTAAACATGG
mlpha gRNA validation (R)	AGTGTTAGACGATGTTAAA
h3f3a gRNA validation (F)	TCTTAGCGGAAGTGGTGCAA
h3f3a gRNA validation (R)	AACAGTTCCGGGCCTGAAAT
downstream_foxd1_deletion_1 (F)	TCACTGAGGCCTCTGACAGA
downstream_foxd1_deletion_2 (R)	TACTCCTTTGGACAGGGCCA
downstream_foxd1_deletion_3 (F)	CTCTGTGGTCTATTTCTCTCC
downstream_foxd1_deletion_4 (R)	CAGAAGGTGAAGCAGCCTCA
downstream_foxd1_deletion_5 (R)	ACCACGTCTTCAAGGGCTTC
fabp10a gRNA validation (F)	ATGGAGGAAAGCTGGTCTGC
fabp10a gRNA validation (R)	TGCTCTTCCTGATCATGGTGG
albino gRNA validation (F)	CGGCTGTTTTTGGAGTGGTG
albino gRNA validation (R)	ACCTTCACCCACCTGTTGTG
wee1 gRNA validation (F)	TGGACTCTCCAGTACCTTTGC
wee1 gRNA validation (R)	GCTCATCCACTAGGTAATGC
mitfa_HDR_detection (F)	GCTACAGTGATGACATTCTTGG
mitfa_HDR_detection (R)	GCATGATTGCTGTACATATCAAGCAAA
tyrp1b_HDR_detection (F)	CGACTGGCCTACAAGGTGAT
typ1b_HDR_detection (R)	CGCCGTCCAGCTCGACCA
h3f3a_HDR_detection (F)	AGGACACGTGCATGAAGTTT
h3f3a_HDR_detection (R)	GAACTTCAGGGTCAGCTTGC
fabp10a_HDR_detection_1 (F)	GGAAGGGCGTGGTCAAGTAT
fabp10a_HDR_detection_1 (R)	GAACTGAGGGGACAGGATG
fabp10a_HDR_detection_2 (F)	GCGAACGATAAAGGTCGCAAG
fabp10a_HDR_detection_2 (R)	CTCTGATGAATAAATACGGC